

Collective expansion in pp collisions using the Tsallis statistics

Jinbiao Gu, Chenyan Li, Qiang Wang, Wenchao Zhang,* and Hua Zheng

School of Physics and Information Technology, Shaanxi Normal University, Xi'an 710119, China

(Dated: January 7, 2022)

We investigate the transverse momentum (p_T) spectra of identified hadrons in minimum-bias proton-proton (pp) collisions at 0.9, 2.76, 5.02, 7 and 13 TeV in the framework of Tsallis-blast wave (TBW) model. In this model, the average radial flow velocity $\langle\beta\rangle$ and the Tsallis temperature T are common for all hadrons, while the degrees of non-equilibrium q are, respectively, universal for mesons and baryons when a combined fit is performed to the p_T spectra of different particles at a given energy. It is found that the model can well describe the particle spectra up to 10 GeV/c. The radial flow velocity increases with the collision energy. The degrees of non-equilibrium and the Tsallis temperature show a similar behaviour, but with a much weaker trend. With the dependence of the freeze-out parameters on the energy, we evaluate $\langle\beta\rangle$, T and q in pp collisions at 8 and 14 TeV and predict the particle spectra at these two energies. We then extend the model to the identified particle spectra at different charged-particle multiplicities in pp collisions at 7 TeV and 13 TeV. It is observed that at both energies the radial flow increases with the multiplicity while the degree of non-equilibrium shows an opposite behaviour, which is similar to that observed in proton-nucleus (pA) and nucleus-nucleus (AA) collisions at the Large Hadron Collider (LHC) energies. However, the Tsallis temperature increases with the multiplicity, which is opposite to the trend in pA and AA collisions. At similar multiplicities, the radial flow in pp collisions is stronger than those in pA and AA collisions, indicating that the size of the colliding system has significant effects on the final state particle dynamics. Finally, we apply an additional flow correction to the Tsallis temperature and found that the thermal temperature almost scales with the multiplicity in a uniform way, despite the difference in the colliding system and the collision energy.

I. INTRODUCTION

Transverse momentum (p_T) spectra of identified particles are fundamental physical observables in high-energy heavy-ion collisions. They are utilized to probe different properties of the produced hot and dense matter, denoted as the quark-gluon plasma (QGP). In the low p_T region ($p_T \lesssim 2$ GeV/c), hadrons are produced from the soft scattering processes and the hadron spectra provide information about the bulk system, such as the kinetic freeze-out temperature T and the collective expansion velocity β . Extraction of these properties relies on the hydrodynamic modelling of the system [1], such as the Boltzmann-Gibbs blast-wave (BGBW) model [2]. In the high p_T region ($p_T \gtrsim 10$ GeV/c), hadrons are generated by hard scatterings of partons with the medium and this process is described by perturbative quantum chromodynamics (pQCD).

The BGBW model has been widely used to describe the hydrodynamical expansion of the produced medium in Au-Au collisions at $\sqrt{s_{NN}} = 7.7$ -200 GeV [3–5], in d-Au collisions at 200 GeV [4], in Pb-Pb collisions at 2.76 and 5.02 TeV [6, 7] and in p-Pb collisions at 5.02 TeV [8]. In proton-proton (pp) collisions at both 7 and 13 TeV, the p_T spectra of identified particles get harder with the increase of the charged-particle multiplicity ($dN_{ch}/d\eta$), with the effect being more obvious for particles with larger mass [9, 10]. This trend is highly similar to that observed in the evolution of the spectra

in proton-nucleus (pA) and nucleus-nucleus (AA) collisions. Thus, the BGBW model is extended to describe the pp collisions [9, 10]. The agreement between the p_T spectra from data and the predictions from the BGBW model indicates that traces of a collective system exist in high multiplicity pp collisions. Moreover, double-ridge structures have also been observed in high multiplicity pp collisions [11]. These collective phenomena are reminiscent to observations attributed to the creation of QGP in Au-Au collisions at the Relativistic Heavy Ion Collider (RHIC), and in Pb-Pb collisions at the Large Hadron Collider (LHC).

In the BGBW model, it assumes that a locally thermalized medium expands with a common radial flow velocity β and then undergoes an instantaneous kinetic freeze-out at the temperature T . However, in AA collisions, the fluctuation of initial conditions for hydrodynamic evolution may not be completely washed out by the subsequent interactions at either the QGP phase or the hadronic phase. In pp collisions, from event to event there is a large energy fluctuation for particle productions. Both of the fluctuations will leave footprints on the particle spectra in the low to intermediate p_T region [12]. Such a situation in AA collisions [13–17] and in pp collisions [18–24] is coped with a non-extensive statistics, i.e., the Tsallis statistics [25]. In order to take both the fluctuation and the collective expansion into account, the Tsallis statistics is embedded into the BGBW model. The Tsallis blast-wave (TBW) model has been utilized to describe the identified particle spectra in Pb-Pb, Xe-Xe and p-Pb collisions at the LHC energies [26] and in Au-Au collisions at the RHIC energies [12, 27, 28]. In Ref. [29], this model is extended to describe the spectra in pp collisions

* wenchao.zhang@snnu.edu.cn

at 0.2, 0.54, 0.9 and 7 TeV. The authors found an onset of radial flow in pp collisions when the energy is above 0.9 TeV.

In this paper, as a complementary study to that performed in Ref. [29], the TBW model is applied to describe the identified particle p_T spectra in minimum-bias [30] pp collisions at 0.9, 2.76, 5.02, 7 and 13 TeV. This study can provide the energy dependence of the radial flow velocity, the kinetic freeze-out temperature as well as the degree of non-equilibrium in small systems. With this dependence, we predict the identified particle spectra in pp collisions at 8 and 14 TeV. Moreover, in order to investigate the multiplicity dependence of the freeze-out parameters, the TBW model is extended to the spectra at different charged-particle multiplicity classes in pp collisions at 7 and 13 TeV. Combined with our previous results in Pb-Pb, Pb-Pb, Xe-Xe and p-Pb collisions at 2.76, 5.02, 5.44 and 5.02 TeV [26], such a systematic study on the multiplicity dependence of radial flow velocity, kinetic freeze-out temperature and the degree of non-equilibrium for different colliding systems at the LHC may shed some light on the possible underlying mechanism for particle productions.

This paper is organized as follows. In sect. II, we briefly introduce the TBW model. In sect. III, results and discussions are presented. Finally, the conclusion is given in sect. IV.

II. THE TBW MODEL

With the recipe of the TBW model in Refs. [12, 26–29], the invariant differential yield of identified particles at mid-rapidity in pp collisions is expressed as [31]

$$\frac{d^2 N}{2\pi p_T dp_T dy} \propto m_T \int_{-y_b}^{+y_b} e^{\sqrt{y_b^2 - y_s^2}} \cosh(y_s) dy_s \int_{-\pi}^{+\pi} d\phi \times \int_0^R r dr \left[1 + \frac{q-1}{T} \left(m_T \cosh(y_s) \cosh(\rho) - p_T \sinh(\rho) \cos(\phi) \right) \right]^{-1/(q-1)}, \quad (1)$$

where

$$m_T = \sqrt{p_T^2 + m^2}, \quad (2)$$

$$y_b = \ln(\sqrt{s}/m_N), \quad (3)$$

$$\rho = \tanh^{-1} \left[\beta_s \left(\frac{r}{R} \right)^n \right]. \quad (4)$$

y , y_s and y_b are, respectively, the rapidities of the produced particle, the emitting source and the beam. m (m_N) is the mass of the produced particle (the colliding nucleon). \sqrt{s} is the center of mass energy. ϕ is the difference between the azimuthal angles of the emitted particle velocity (ϕ_b) and the boost of the source element

(ϕ_b) with respect to the reaction plane. ϕ_b is deemed as the same as the azimuthal angle of the source element in coordinate space, ϕ_s . T is the Tsallis temperature, q is a non-extensive parameter which describes the deviation of the system from thermal equilibrium. As described in Ref. [32], the Tsallis distribution is interpreted as a superposition of Boltzmann-Gibbs distributions with different temperatures. The fluctuation of these temperatures is given by the deviation of q from unity, while the average value of their reciprocals represents $1/T$. When $q \rightarrow 1$, one recovers the distribution in the BGBW model. ρ is the transverse flow rapidity growing as the n th power of the radial distance (r) in the transverse plane. β_s is the transverse flow velocity at the surface of the fireball ($r = R$). The average transverse flow velocity is expressed as $\langle \beta \rangle = 2/(n+2)\beta_s$. In the model, the default value of n is set as 1 and $\langle \beta \rangle = 2/3\beta_s$. In our recent paper, we found that in central AA collisions the freeze-out parameters rely on the choice of n [26]. In this paper, in order to investigate whether a similar dependence emerges in pp collisions, besides the linear velocity profile, a constant velocity profile with $n = 0$ [33] is also considered. This profile was first applied in the description of the identified particle's elliptic flow in Au-Au collisions with the BGBW model [34]. For both transverse velocity profiles, four free parameters are to be extracted: the normalization constant, $\langle \beta \rangle$, q and T .

III. RESULTS AND DISCUSSIONS

The ALICE collaboration has presented a series of identified particle spectra in pp collisions at 0.9, 2.76, 5.02 [35], 7 and 13 TeV [36–47]. Recently, they also published the spectra with different charged-particle multiplicity classes in pp collisions at 7 and 13 TeV [9, 10, 48–50]. Table I shows the references for the spectra of identified particles at a given energy. Here, π , K , p , K^{*0} , Λ , Ξ and Ω , respectively, refer to $\pi^+ + \pi^-$, $K^+ + K^-$, $p + \bar{p}$, $K^{*0} + \bar{K}^{*0}$, $\Lambda + \bar{\Lambda}$, $\Xi^- + \bar{\Xi}^+$ and $\Omega^- + \bar{\Omega}^+$.

TABLE I. Summary of references for the identified particle spectra at a given energy.

	π, K, p	K^{*0}, ϕ	$K_S^0, \Lambda, \Xi, \Omega$
0.9 TeV	[36]	[37] ^a	[37]
2.76 TeV	[38]	[39]	[40, 41]
5.02 TeV	[42]	[43]	[44]
7 TeV	[9, 42]	[9, 45]	[9, 46–48]
13 TeV	[10, 46]	[46, 49]	[46, 50]

^a For pp collisions at 0.9 TeV, the spectra of K^{*0} and Ω are not yet available.

In order to investigate the evolution of the freeze-out parameters as a function of the collision energy, a combined fit is performed to the identified particle spectra with the TBW model in minimum-bias pp collisions at a given energy using a least χ^2 method. At low p_T , for

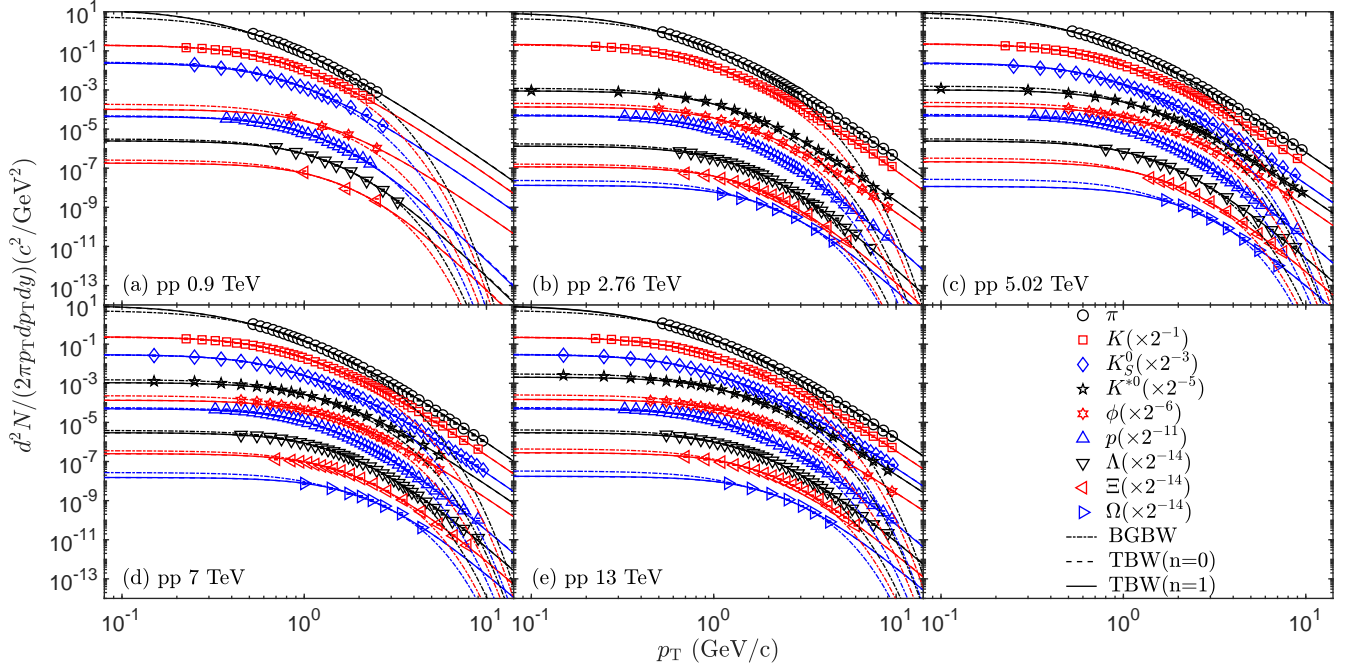


FIG. 1. (Colour online) Identified particle p_T spectra in pp collisions at 0.9 TeV (a), 2.76 TeV (b), 5.02 TeV (c), 7 TeV (d) and 13 TeV (e). The symbols are experimental data taken from Refs. [36–47]. The solid (dash) curves represent the results from the TBW model with the linear (constant) velocity profile, while the dash-dotted lines are the results from the BGBW model.

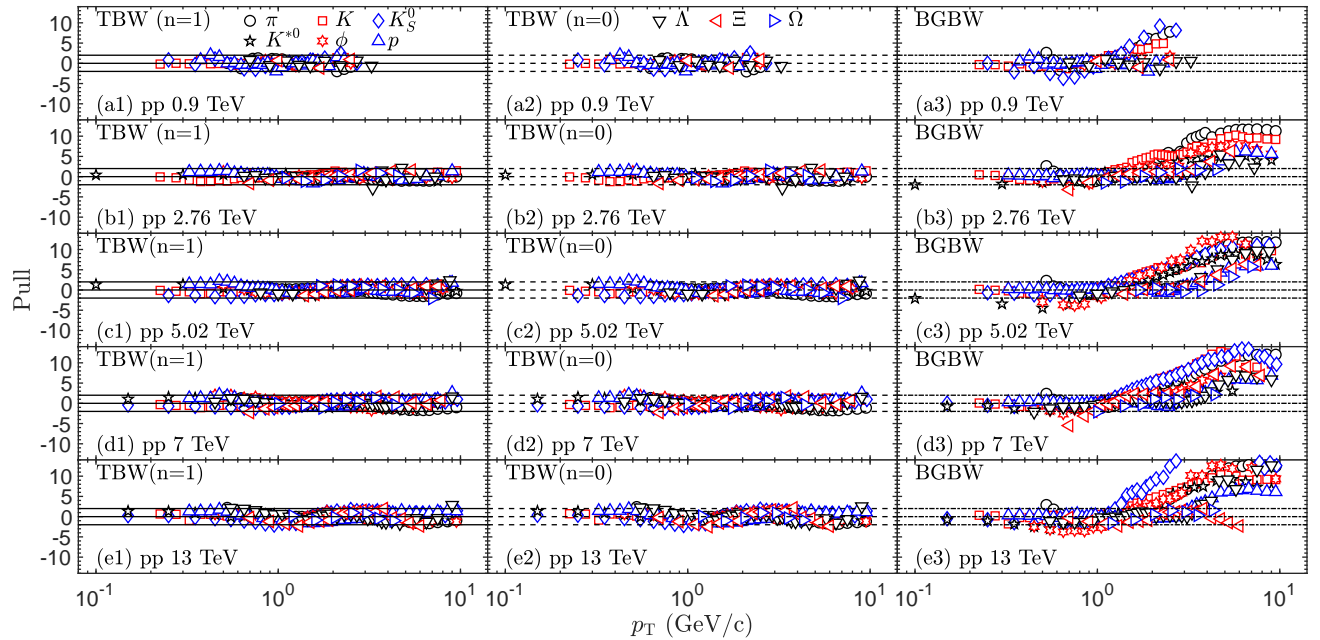


FIG. 2. (Colour online) The pull distributions for the TBW model with $n = 1$ (left column), $n = 0$ (middle column) and the BGBW model (right column) in pp collisions at 0.9, 2.76, 5.02, 7 and 13 TeV from top to bottom panels. In a given subfigure, the upper and lower solid, dash or dash-dotted lines represent that the deviation between the model and the data is 2 times of the data's error.

pions there is a large feed-down contribution from resonance decays, which will steepen the spectra [6]. To remove this contribution, the pion spectrum at the low p_T region ($p_T < 0.5$ GeV/c) is excluded from the fit. This cut has been widely used in the BGBW parameterization of the particle spectra in AA and pp collisions by experimental groups [3–10]. In the fit, the average flow velocity $\langle\beta\rangle$ and the Tsallis temperature T are common for all hadrons, while the degrees of non-equilibrium are, respectively, universal for the meson group (q_M) and the baryon group (q_B). It is found that the separation of mesons and baryons shows good fits while one single q for all particles gives a bad description of the spectra. In addition, different particles own different normalization factors and masses. The freeze-out parameters of the combined TBW fit in pp collisions at the given energy are tabulated in Table II. Also shown in the table are the χ^2 values divided by the number of degrees of freedom (χ^2/NDF). The first uncertainty in the table is the statistical error returned from the combined fit. The second one is the systematic uncertainty which is due to the variation of the lower bound (from 0.5 to 0.1 GeV/c) for the pion spectrum. Fig. 1(a) ((b), (c), (d) and (e)) presents the identified particle spectra with their associated TBW model results in pp collisions at 0.9 (2.76, 5.02, 7 and 13) TeV. At each energy, in a logarithmic scale the curves from the model with both $n = 1$ (solid lines) and $n = 0$ (dash lines) well describe the data over a broad p_T range (0-10 GeV/c). In order to quantify the agreement between the data points and the fitted curves, a variable pull=(data-fitted)/ Δ data [51] is evaluated. The pull distributions in the left and middle columns of Fig. 2 show that most of the data are consistent with the TBW model within 2 standard deviations. As a comparison, the BGBW calculations (dash-dotted lines) are also presented in Fig. 1. As the average transverse flow velocity and the kinetic freeze-out temperature of the BGBW model for minimum-bias pp collisions are not available so far in literature, they are determined by fitting the model simultaneously to the spectra of charged pions, kaons and protons in the ranges 0.5-1 GeV/c, 0.2-1.5 GeV/c and 0.3-3 GeV/c, respectively. The choice of particle species as well as the BGBW fit range is consistent with the previous publications of the ALICE collaboration [9, 10]. As can be seen from the Figs. 1 and 2, in the high p_T region the BGBW model tends to underestimate the particle spectra and a large deviation between the data and the fitted curves is observed.

With the parameters in Table II, we present the dependence of $\langle\beta\rangle$, T , q_B and q_M for the TBW model on the collision energy in Fig. 3. Also shown in the figure are the freeze-out parameters for the BGBW model. The solid curves represent logarithmic parameterizations of the dependence. Some results can be obtained from the figure as follows.

(i) The freeze-out parameters from the TBW model with $n = 1$ are consistent with those from the model with $n = 0$ within uncertainties, which indicates that for

minimum-bias pp collisions the results have little dependence on the choice of the transverse velocity profile.

(ii) For the TBW model, the average transverse flow velocity $\langle\beta\rangle$ grows with the energy. The growth can be parameterized as $\langle\beta\rangle = (0.202 \pm 0.026) + (0.035 \pm 0.014) \ln(\sqrt{s}/\text{TeV})$. Similar trend was observed in minimum-bias pp collisions at lower energies [29] and in central Au-Au collisions at the RHIC energies [5, 27]. It is interpreted as a possible indication of a more rapid expansion with increasing energy. This is consistent with the expectation that a shorter-lived medium in pp collisions at lower energy has less time to build up radial flow. In pp collisions at 13 TeV, $\langle\beta\rangle$ reaches an average value of $0.307 \pm 0.007 \pm 0.028$, which is comparable with that in peripheral (60-80%) Pb-Pb collisions at 2.76 TeV, $0.293 \pm 0.012 \pm 0.014$ [26].

(iii) Compared to $\langle\beta\rangle$, the Tsallis temperature T shows a similar but much weaker dependence on the energy, which is described by $T = (0.070 \pm 0.006) + (0.008 \pm 0.004) \ln(\sqrt{s}/\text{TeV})$. This dependence is similar to that observed in Refs. [54, 55] and could be argued as follows [56]. In pp collisions at lower energy, particles decouple earlier from the medium, which seems to freeze out at a higher temperature. However, the initial temperature of the medium is smaller, as less energy is deposited in the interacting system. This will lead to a lower temperature at lower energy.

(iv) Both of the non-extensive parameters q_M and q_B show a weak increase with the energy. This trend is similar to that observed in pp collisions at lower energy [29] and in peripheral Au-Au collisions [27]. The increase can be separately described as $q_M = (1.1190 \pm 0.0028) + (0.0042 \pm 0.0016) \ln(\sqrt{s}/\text{TeV})$ and $q_B = (1.0949 \pm 0.0005) + (0.0039 \pm 0.0003) \ln(\sqrt{s}/\text{TeV})$. It means that the system is more out of equilibrium toward higher energy. A possible explanation for this trend is that as the energy increases the initial state energy fluctuation due to colour glass condensate formation becomes more obvious [27].

(v) At a given energy, q_M is larger than q_B . Similar conclusions are obtained in pp collisions at lower energy [29]. This could be explained as follows. At high- p_T , the particle spectrum behaves as a power law distribution, p_T^{-n} . The index n is related to the non-extensive parameter q with $n = 1/(q - 1)$. As shown in Refs. [57, 58], n is expressed as $n = 2n_a - 4$, where n_a is the number of active participating quarks. If the dominate processes for the hadron productions are parton-parton hard scatterings $qq \rightarrow qq$ (referred as the leading twist process), then the counting rule will give $n = 4$. The index n will become larger if the contribution from higher twist processes is taken into account. For example, for the meson scattering process $q + \text{meson} \rightarrow q + \text{meson}$, $n = 8$, while for the baryon scattering process $q + \text{baryon} \rightarrow q + \text{baryon}$, $n = 12$. n is larger for baryons than mesons, which implies that the higher twist process prefers the baryon production than the meson production.

(vi) The average transverse flow velocity $\langle\beta\rangle$ is larger

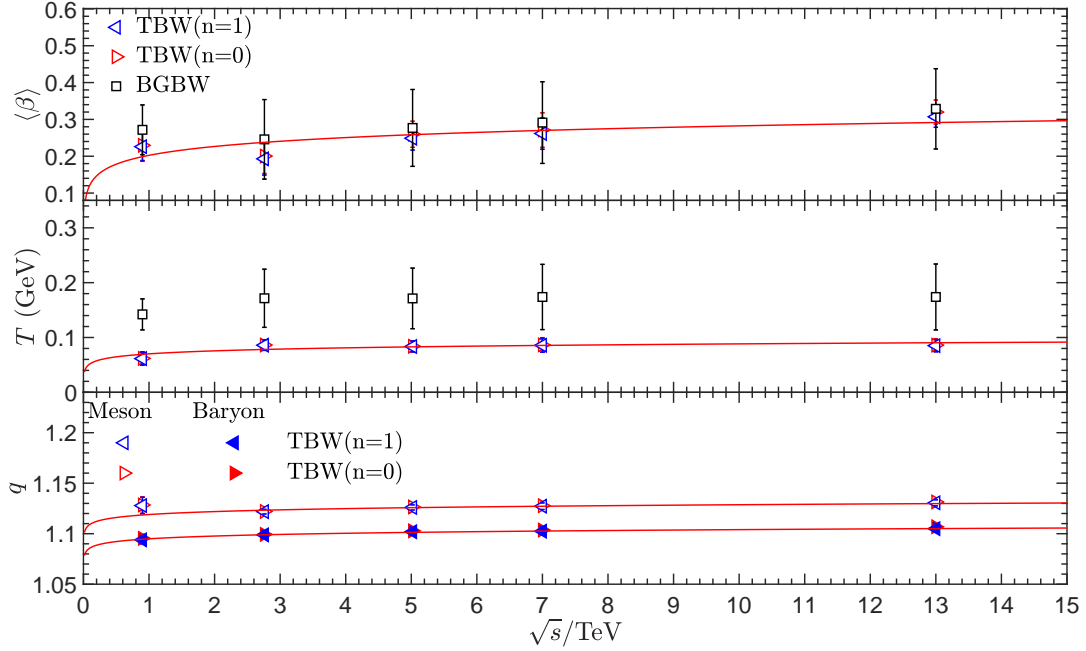


FIG. 3. (Colour online) $\langle\beta\rangle$, T , q_M and q_B as a function \sqrt{s}/TeV . The solid curves represent a logarithmic fit for the dependence of the freeze-out parameters on the collision energy.

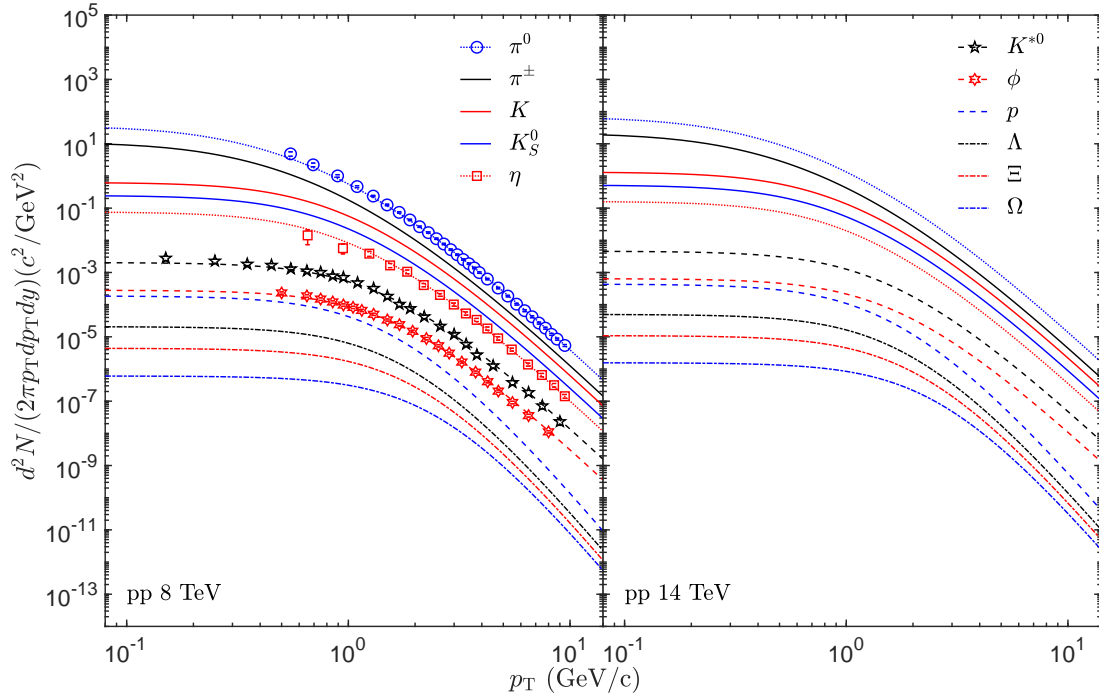


FIG. 4. (Colour online) Identified particle p_T spectra in pp collisions at 8 TeV (the left panel) and 14 TeV (the right panel). The solid, dash, dash-dotted and dotted curves represent the spectra predicted from the TBW model. The different symbols in the left panel are the experimental spectra of π^0 , η , K^{*0} and ϕ [52, 53].

in the BGBW model than in the TBW model. Moreover, the kinetic freeze-out temperature in the former is higher than the Tsallis temperature in the latter. It seems that the BGBW model has translated the non-equilibrium effects into nonzero radial flow velocity and higher temperature [12].

With the parameterization of the freeze-out parameters on the energy, we could evaluate $\langle\beta\rangle$, T and q in pp collisions at 8 TeV and 14 TeV. For the former, $\langle\beta\rangle=0.275$, $T = 0.087$ GeV, $q_M = 1.1278$ and $q_B = 1.1031$, while for the later, $\langle\beta\rangle=0.294$, $T = 0.091$ GeV, $q_M = 1.1301$ and $q_B = 1.1054$. With these values, we can predict the spectra of identified particles in pp collisions at these two energies. The solid, dash, dash-dotted and dotted curves in Fig. 4 represent the predicted spectra. Also shown in the figure are the experimental spectra of π^0 , η , K^{*0} and ϕ in pp collisions at 8 TeV [52, 53]. It is observed that the predicted curves well describe the data points of these four identified particles, which implies that our prediction of the p_T spectra from the TBW model is reliable.

In order to investigate the multiplicity dependence of the freeze-out parameters, we extend the investigation to the identified particle spectra with different charged-particle multiplicity classes [59] in pp collisions at 7 TeV and 13 TeV. For the spectra at the multiplicity classes IX and X (class X) in pp collisions at 7 (13) TeV, $\langle\beta\rangle$ returned from the combined fit is as low as 10^{-5} . Thus we fix it as 0 and repeat the analyses. Fig. 5 shows the identified particle spectra together with the TBW results at two selected multiplicity classes (classes I and X) for these two energies. At each energy, the TBW model generally reproduces the data at both multiplicity classes well. Also shown in the figure are the BGBW results with $\langle\beta\rangle$ and T taken from Refs. [9, 10]. As can be seen from Fig. 6, the agreement between the data and the TBW model results is within 2 standard deviations. However, for the BGBW model the data is underestimated at high p_T , which is similar to that in minimum-bias pp collisions. The TBW fit parameters and χ^2/NDF for different multiplicity classes in pp collisions at 7 and 13 TeV are, respectively, summarized in Tables III and IV. With these parameters, we present the correlation between $\langle\beta\rangle$ and T in Fig. 7. As a comparison, the correlation of the parameters in Pb-Pb (Pb-Pb, Xe-Xe, p-Pb) collisions at 2.76 (5.02, 5.44, 5.02) TeV is also shown in the figure [26]. It is found that the evolution of T with $\langle\beta\rangle$ in pp collisions at 13 TeV follows a similar trend as the one observed at 7 TeV, namely T growing with $\langle\beta\rangle$ until it reaches a saturation. Obviously, this trend is opposite to that in pA and AA collisions. Moreover, it is different to the one observed in the BGBW model, in which T non-monotonically depends on $\langle\beta\rangle$ [10]. In addition, the dependence of $\langle\beta\rangle$, T and q on $\langle dN_{\text{ch}}/d\eta\rangle$ for the TBW model in different colliding systems [60] is illustrated in Fig. 8. Also presented in the figure is the evolution of $\langle\beta\rangle$ and T for the BGBW model in pp collisions at 7 and 13 TeV. Several conclusions can be drawn from the figure.

(i) $\langle\beta\rangle$, T and q for the TBW model with $n = 1$ are, respectively, in agreement with those from the model with $n = 0$ within errors at low multiplicities. However, at large multiplicities, deviation appears and it becomes more obvious with increasing $\langle dN_{\text{ch}}/d\eta\rangle$. It might mean that the freeze-out parameters at large $\langle dN_{\text{ch}}/d\eta\rangle$ are sensitive to the choice of the transverse velocity profile.

(ii) $\langle\beta\rangle$ increases with $\langle dN_{\text{ch}}/d\eta\rangle$ and the values of $\langle\beta\rangle$ for pp collisions at different energies are in agreement within error bars, indicating that the small system becomes more explosive at larger multiplicities. In the common $\langle dN_{\text{ch}}/d\eta\rangle$ range, $\langle\beta\rangle$ is higher in pp collisions than in pA and AA collisions, while the Tsallis temperature in the former is lower than the latter. This indicates that the size of the colliding system has significant effects on the final state particle dynamics. In pp collisions, the initial energy density is higher than that in pA or AA collisions, resulting a stronger radial flow gradient and a lower freeze-out temperature [9, 61].

(iii) The non-extensive parameter q decreases with the increase of $\langle dN_{\text{ch}}/d\eta\rangle$, indicating that the system is approaching thermal equilibrium at high multiplicities. For pp collisions, both q_M and q_B will reach a saturation at low multiplicities. Moreover, at a given multiplicity, q_M is larger than q_B , which is similar to that observed in minimum-bias pp collisions.

(iv) The Tsallis temperature in pA and AA collisions decreases with the increase of $\langle dN_{\text{ch}}/d\eta\rangle$. However, in pp collisions it exhibits an opposite behaviour and becomes saturate at high multiplicities, which is in contrast to the expectation that at larger multiplicities the system is longer-lived and thus the freeze-out temperature should be smaller. This is not understood in the present work. Moreover, in pp collisions, the Tsallis temperature is obviously lower than the kinetic freeze-out temperature in the BGBW model, which is similar to the observation in minimum-bias pp collisions.

Finally, as described in Ref. [26], due to the existence of a radial flow, the thermal temperature [62] at the light hadrons freeze-out is larger than the original Tsallis temperature by a blue shift factor, $T_{\text{th}} = T\sqrt{(1 + \langle\beta\rangle)/(1 - \langle\beta\rangle)}$. This is similar to the case in the BGBW model [2]. Fig. 9 shows the dependence of the thermal temperature for the TBW model with $n = 1$ in pp, pA and AA collisions. As a comparison, the Tsallis temperature is also presented in the figure. For a given system at a certain collision energy, the thermal temperature increases with the multiplicity, showing a similar trend as the average transverse momentum [6, 8–10, 63]. Moreover, it is systematically larger than the Tsallis temperature, except for the multiplicities where the average transverse flow is 0. As $\langle\beta\rangle$ increases with the multiplicities, the blue shift factor shows a similar behaviour, leading to a more obvious difference between these two temperatures at higher multiplicities. Finally, despite the difference in the colliding system and the collision energy, T_{th} almost scales with the multiplicity in a uniform way, indicating that a universal particle produc-

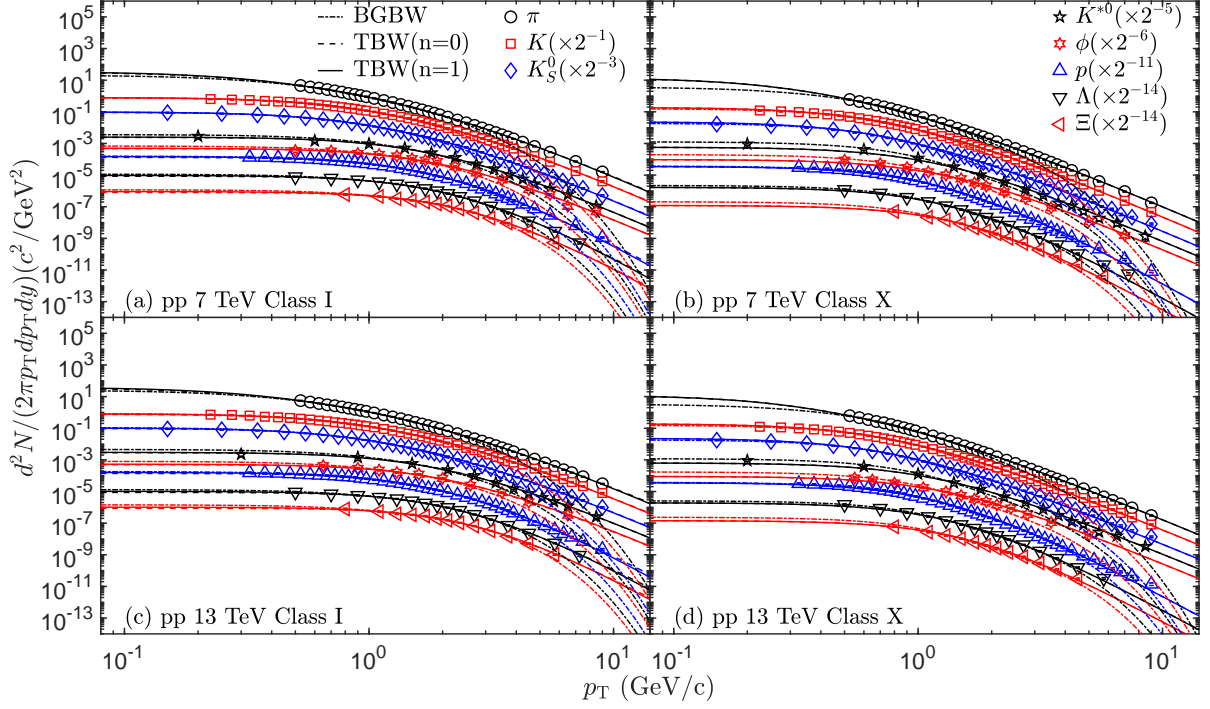


FIG. 5. (Colour online) Identified particle p_T spectra at the multiplicity class I (left column) and class X (right column) in pp collisions at 7 and 13 TeV from top to bottom panels. The symbols are experimental data taken from Refs. [9, 10, 48–50]. The solid (dash) curves represent the results from the TBW model with the linear (constant) velocity profile, while the dash-dotted lines are the results from the BGBW model.

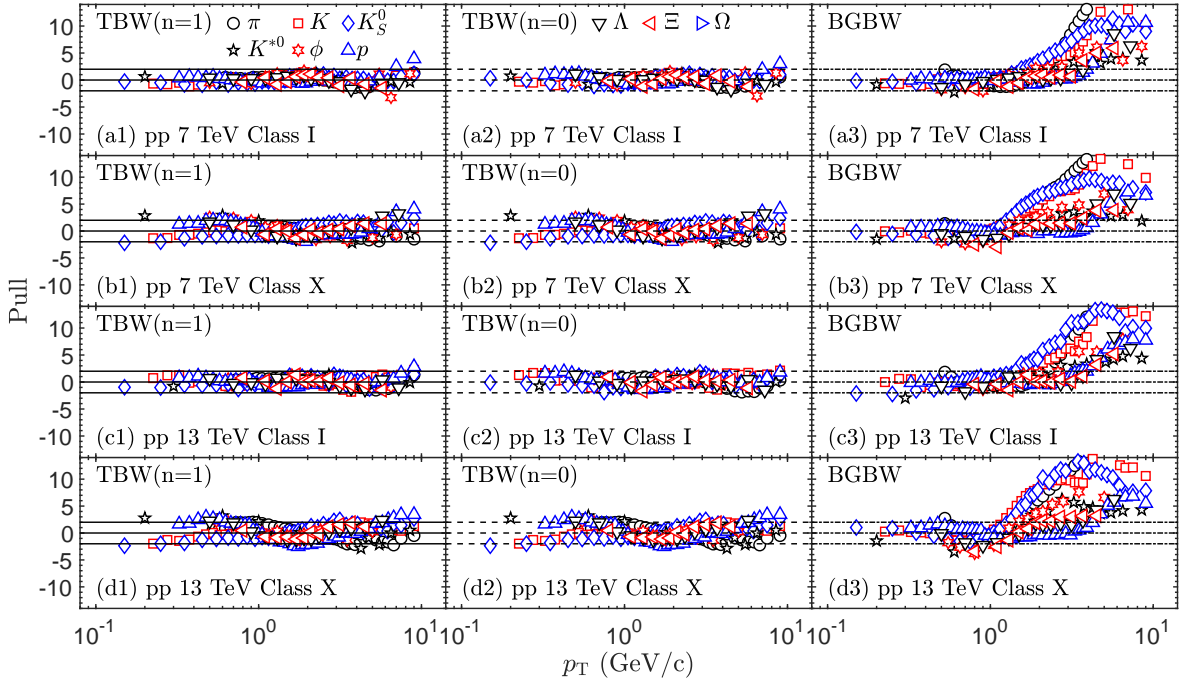


FIG. 6. (Colour online) The pull distributions for the TBW model with $n = 1$ (left column), $n = 0$ (middle column) and the BGBW model (right column) at the multiplicity classes I and X in pp collisions at 7 and 13 TeV from top to bottom panels. In a given subfigure, the upper and lower solid, dash or dash-dotted lines represent that the deviation between the model and the data is 2 times of the data's error.

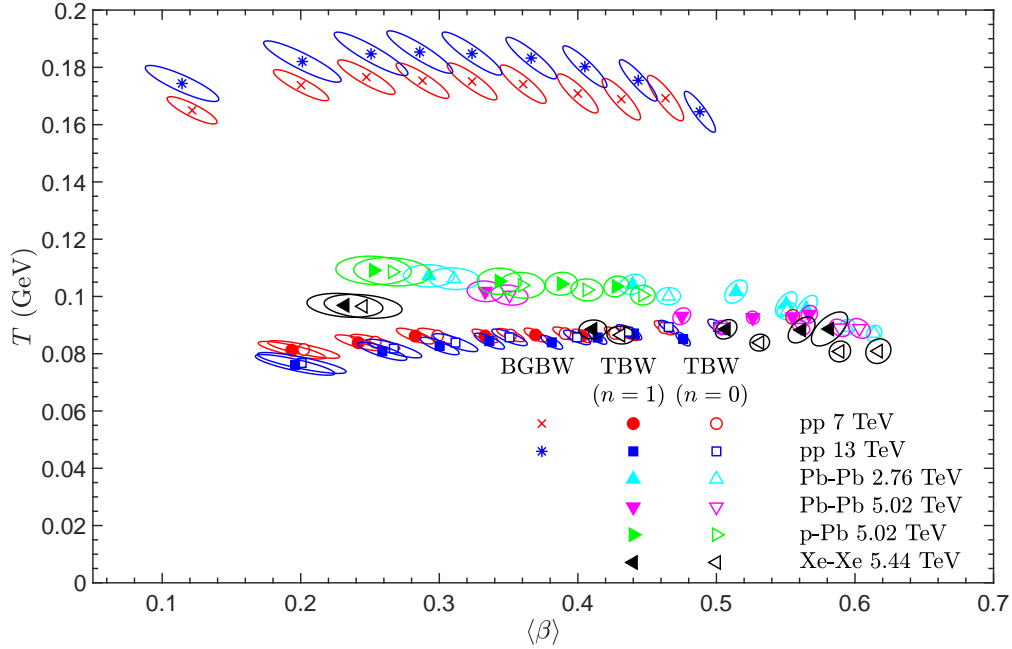


FIG. 7. (Colour online) Correlation of the Tsallis temperature T and the average transverse flow velocity $\langle\beta\rangle$ for the TBW model in pp (pp, Pb-Pb, Xe-Xe, p-Pb) collisions at 7 (13, 2.76, 5.02, 5.44, 5.02) TeV. Also shown in the figure are the correlations between T and $\langle\beta\rangle$ for the BGBW model in pp collisions at 7 and 13 TeV. The elliptic contours reflect 1σ uncertainty. The charged-particle multiplicity increases from left to right for a given colliding system at a selected energy.

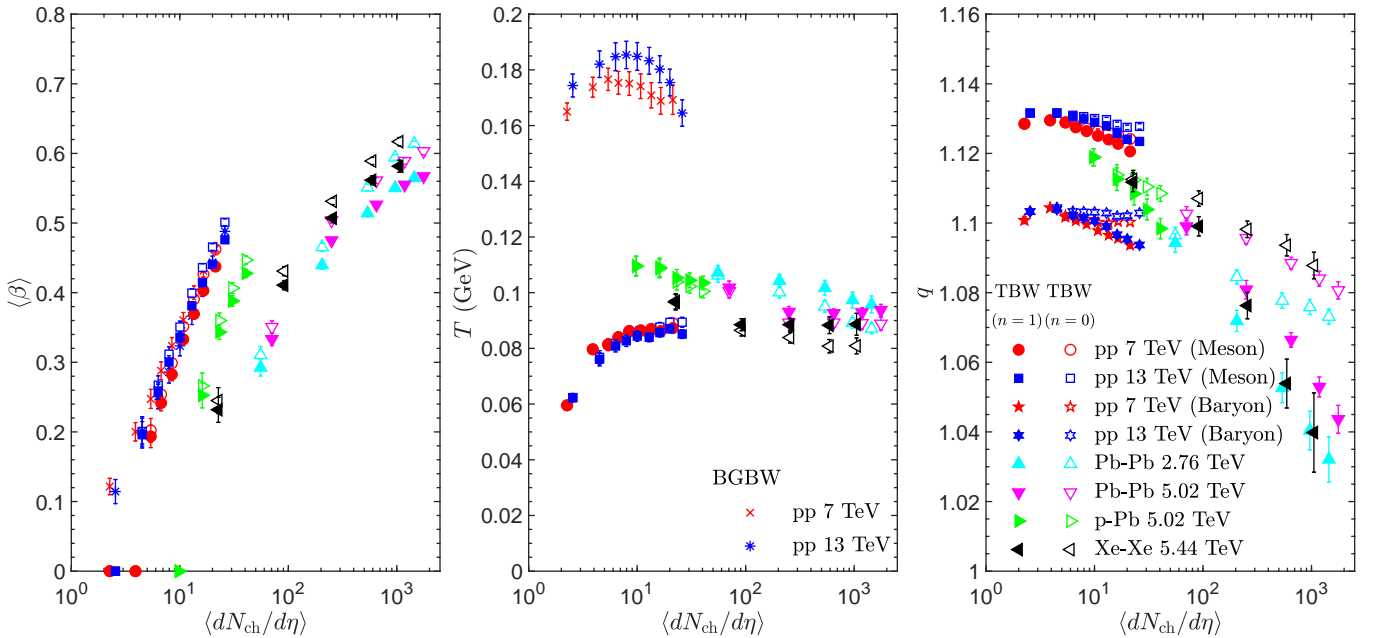


FIG. 8. (Colour online) The dependence of $\langle\beta\rangle$, T and q on $\langle dN_{ch}/d\eta\rangle$ for the TBW model in pp (pp, Pb-Pb, Xe-Xe, p-Pb) collisions at 7 (13, 2.76, 5.02, 5.44, 5.02) TeV. Also shown in the figure is the evolution of $\langle\beta\rangle$ and T with $\langle dN_{ch}/d\eta\rangle$ for the BGBW model in pp collisions at 7 and 13 TeV.

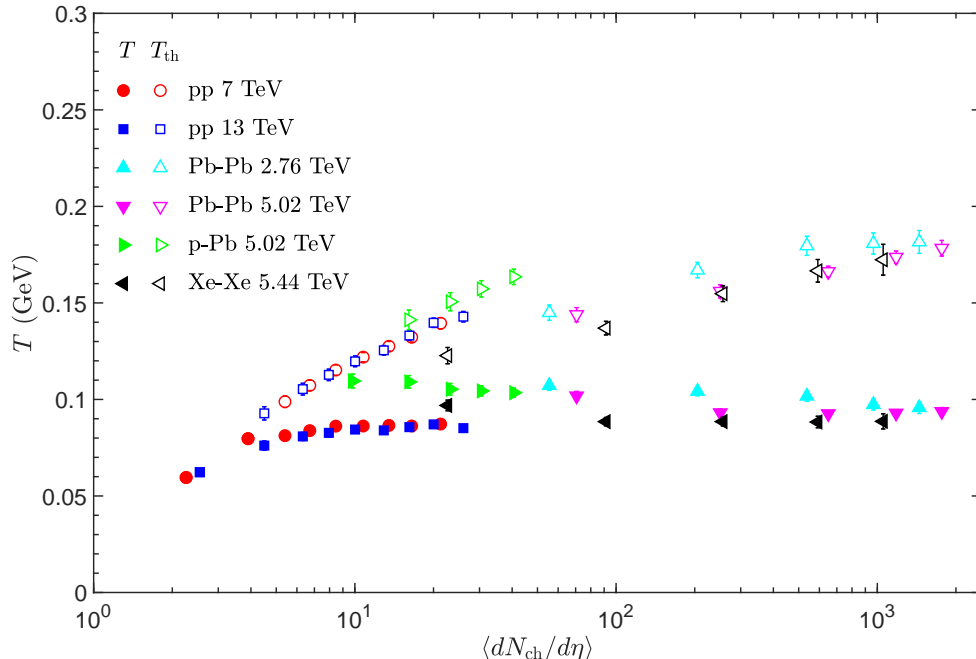


FIG. 9. (Colour online) The thermal as well as the Tsallis temperature for the TBW model with $n = 1$ as a function of $\langle dN_{ch}/d\eta \rangle$ for identified hadrons in pp (pp, Pb-Pb, Xe-Xe, p-Pb) collisions at 7 (13, 2.76, 5.02, 5.44, 5.02) TeV.

tion mechanism may exist in pp, pA and AA collisions at the LHC energies.

IV. CONCLUSIONS

In this paper, in order to investigate the evolution of the freeze-out parameters as a function of the collision energy, we have used the Tsallis blast-wave model to simultaneously fit the identified hadron p_T in minimum-bias pp collisions at 0.9, 2.76, 5.02, 7 and 13 TeV. In the combined fit, the Tsallis temperature and the average radial flow velocity are common for all hadrons, while the degrees of non-equilibrium are, respectively, universal for mesons and baryons. We find that the model can well describe the hadron spectra up to 10 GeV/c. The radial flow velocity grows with the increase of the collision energy. The degrees of non-equilibrium and the Tsallis temperature exhibit a similar behaviour as the radial flow velocity, but with a much weaker trend. With the parameterization of the freeze-out parameters on the energy, $\langle \beta \rangle$, T and q in pp collisions at 8 and 14 TeV are evaluated and the particle spectra at these two energies are predicted. The agreement between the predicted curves and the experimental data of π^0 , η , K^{*0} and ϕ in pp collisions at 8 TeV implies that our prediction of the p_T spectra from the TBW model is reliable. In order to investigate the multiplicity dependence of the freeze-out parameters, the model is extended to the identified particle spectra at different charged-particle multiplici-

ties in pp collisions at 7 TeV and 13 TeV. It is observed that at both energies the radial flow increases with the multiplicity while the degree of non-equilibrium shows an opposite behaviour, which is similar to that observed in pA and AA collisions at the LHC energies. However, the Tsallis temperature increases with the multiplicity, which is opposite to the trend in pA and AA collisions. At similar multiplicities, the radial flow in pp collisions is larger than those in pA and AA collisions, indicating that the size of the colliding system has significant effects on the final state particle dynamics. Moreover, we find that for minimum-bias pp collisions as well as pp collisions at low multiplicities the freeze-out parameters have little dependence on the choice of the transverse velocity profile. However, for pp collisions at high multiplicities these parameters are sensitive to the choice of n in the TBW model. Finally, to obtain the thermal temperature, an additional flow correction is applied to the Tsallis temperature. Despite the difference in the colliding system and the collision energy, the thermal temperature depends on the multiplicity in a similar manner, indicating that a common particle production mechanism may exist in pp, pA and AA collisions at the LHC energies.

ACKNOWLEDGMENTS

We wish to thank the ALICE and CMS collaborations for their share of the experimental data. This work is supported by the Fundamental Research Funds for the Cen-

tral Universities of China under GK202003019, by the Scientific Research Foundation for the Returned Overseas Chinese Scholars, State Education Ministry, by Natural Science Basic Research Plan in Shaanxi Province of China (program No. 2020JM-289) and by the National Natural Science Foundation of China under Grant Nos. 11447024, 11505108, 11905120 and 11947416.

Appendix

The freeze-out parameters in minimum-bias pp collisions and in pp collisions at a given multiplicity class are

summarized in Tables II to IV. Moreover, we tabulate the values of $\langle dN_{\text{ch}}/d\eta \rangle$ at different multiplicity classes in pp collisions and different centralities in pA and AA collisions, respectively, in Tables V and VI.

-
- [1] R. de Souza *et al.*, Prog. Part. Nucl. Phys. **86**, 35 (2016).
 [2] E. Schnedermann, J. Sollfrank, and U. Heinz, Phys. Rev. C **48**, 2462 (1993).
 [3] J. Adam *et al.* (ALICE Collaboration), Phys. Rev. Lett. **92**, 112301 (2004).
 [4] B. Abelev *et al.* (ALICE Collaboration), Phys. Rev. C **79**, 034909 (2009).
 [5] B. Abelev *et al.* (ALICE Collaboration), Phys. Rev. C **96**, 044904 (2017).
 [6] B. Abelev *et al.* (ALICE Collaboration), Phys. Rev. C **88**, 044910 (2013).
 [7] S. Acharya *et al.* (ALICE Collaboration), Phys. Rev. C **101**, 044907 (2020).
 [8] B. Abelev *et al.* (ALICE Collaboration), Phys. Lett. B **728**, 25 (2014).
 [9] S. Acharya *et al.* (ALICE Collaboration), Phys. Rev. C **99**, 024906 (2019).
 [10] S. Acharya *et al.* (ALICE Collaboration), Eur. Phys. J. C **80**, 693 (2020).
 [11] G. Aad *et al.* (ATLAS Collaboration), Phys. Rev. Lett. **116**, 172301 (2016).
 [12] Z. Tang *et al.*, Phys. Rev. C **79**, 051901(R) (2009).
 [13] J. Adams *et al.* (STAR Collaboration), Phys. Lett. B **637**, 161 (2006).
 [14] A. Adare *et al.* (PHENIX Collaboration), Phys. Rev. C **83**, 024909 (2011).
 [15] S. Chatrchyan *et al.* (ALICE Collaboration), Eur. Phys. J. C **74**, 2847 (2014).
 [16] M. D. Azmi and J. Cleymans, Acta Phys. Pol. B Proc. Suppl. **7**, 9 (2014).
 [17] H. Zheng and L. Zhu, Adv. High Energy Phys. **2015**, 180491 (2015).
 [18] J. Cleymans and D. Worku, J. Phys. G: Nucl. Part. Phys. **39**, 025006 (2012).
 [19] J. Cleymans *et al.*, Phys. Lett. B **723**, 351 (2013).
 [20] M. D. Azmi and J. Cleymans, J. Phys. G: Nucl. Part. Phys. **41**, 065001 (2014).
 [21] M. D. Azmi and J. Cleymans, Eur. Phys. J. C **75**, 430 (2015).
 [22] L. Marques *et al.*, Phys. Rev. D **91**, 054025 (2015).
 [23] H. Zheng *et al.*, Phys. Rev. D **92**, 074009 (2015).
 [24] A. Khuntia *et al.*, Eur. Phys. J. A **53**, 103 (2017).
 [25] C. Tsallis, J. Stat. Phys. **52**, 479 (1988).
 [26] G. Che *et al.*, J. Phys. G: Nucl. Part. Phys. **48**, 095103 (2021).
 [27] J. Chen *et al.*, Phys. Rev. C **104**, 034901 (2021).
 [28] M. Shao *et al.*, J. Phys. G: Nucl. Part. Phys. **37**, 085104 (2010).
 [29] K. Jiang *et al.*, Phys. Rev. C **91**, 024910 (2015).
 [30] In order to distinguish the spectra with and without the multiplicity cut in pp collisions, the phrase "minimum-bias" is introduced for the latter.
 [31] The derivation of this formula can be found in the appendix of our previous paper [26].
 [32] G. Wilk and Z. Wlodarczyk, Phys. Rev. Lett. **84**, 2770 (2000).
 [33] In the constant profile, $\langle \beta \rangle = \beta_s$.
 [34] C. Adler *et al.* (STAR Collaboration), Phys. Rev. Lett. **87**, 182301 (2001).
 [35] The spectra of strange particles in pp collisions at 5.02 TeV were published by the CMS collaboration.
 [36] K. Aamodt *et al.* (ALICE Collaboration), Eur. Phys. J. C **71**, 1655 (2011).
 [37] K. Aamodt *et al.* (ALICE Collaboration), Eur. Phys. J. C **71**, 1594 (2011).
 [38] B. Abelev *et al.* (ALICE Collaboration), Phys. Lett. B **736**, 196 (2014).
 [39] J. Adam *et al.* (ALICE Collaboration), Phys. Rev. C **95**, 064606 (2017).
 [40] D. Colella (for the ALICE Collaboration), J. Phys. Conf. Ser. **509**, 012090 (2014).
 [41] L. Hanratty, Ph.D. thesis, Birmingham U. (2014).
 [42] J. Adam *et al.* (ALICE Collaboration), Phys. Lett. B **760**, 720 (2016).
 [43] S. Acharya *et al.* (ALICE Collaboration), Phys. Lett. B **802**, 135225 (2020).
 [44] A. M. Sirunyan *et al.* (CMS Collaboration), Phys. Rev. C **101**, 064906 (2020).
 [45] S. Acharya *et al.* (ALICE Collaboration), Phys. Rev. C **102**, 024912 (2020).
 [46] S. Acharya *et al.* (ALICE Collaboration), Eur. Phys. J. C **81**, 256 (2021).
 [47] B. Abelev *et al.* (ALICE Collaboration), Phys. Lett. B **712**, 309 (2012).
 [48] J. Adam *et al.* (ALICE Collaboration), Nature Phys. **13**, 535 (2017).
 [49] S. Acharya *et al.* (ALICE Collaboration), Phys. Lett. B **807**, 135501 (2020).
 [50] S. Acharya *et al.* (ALICE Collaboration), Eur. Phys. J. C **80**, 167 (2020).

- [51] Δ data is square root of the quadratic sum of the data's statistical and systematic uncertainties.
- [52] S. Acharya *et al.* (ALICE Collaboration), *Eur. Phys. J. C* **78**, 263 (2018).
- [53] S. Acharya *et al.* (ALICE Collaboration), *Phys. Rev. C* **102**, 024912 (2020).
- [54] H. L. Lao *et al.*, *Eur. Phys. J. A* **53**, 44 (2017).
- [55] H. L. Lao *et al.*, *Nucl. Sci. Tech.* **29**, 82 (2018).
- [56] However, in some literatures the authors claimed that the kinetic freeze-out temperature showed decreasing trend [5, 66] or little dependence with the increase of the energy [65, 67].
- [57] P. K. Khandai *et al.*, *Int. J. Mod. Phys. A* **28**, 1350066 (2013).
- [58] C. Y. Wong and G. Wilk, *Phys. Rev. D* **87**, 114007 (2013).
- [59] The values of $\langle dN_{\text{ch}}/d\eta \rangle$ at different multiplicity classes in pp collisions can be found in Table V.
- [60] The values of $\langle dN_{\text{ch}}/d\eta \rangle$ at different centralities in pA and AA collisions can be found in Table VI.
- [61] E. Shuryak and I. Zahed, *Phys. Rev. C* **88**, 044915 (2013).
- [62] It is defined as the inverse slope at high m_T or p_T . The derivation of T_{th} in the TBW model can be found in the appendix of Ref. [26].
- [63] S. Acharya *et al.* (ALICE Collaboration), *Eur. Phys. J. C* **81**, 584 (2021).
- [64] S. Acharya *et al.* (ALICE Collaboration), *Phys. Lett. B* **790**, 35 (2019).
- [65] B. Abelev *et al.* (ALICE Collaboration), *Phys. Rev. Lett.* **109**, 252301 (2012).
- [66] S. Zhang *et al.*, *Adv. High Energy Phys.* **2016**, 9414239 (2016).
- [67] A. Andronic, *Int. J. Mod. Phys. A* **29**, 1430047 (2014).

TABLE II. Summary of the freeze-out parameters for the TBW model and the BGBW model in pp collisions at 0.9, 2.76, 5.02, 7 and 13 TeV. The first error is returned from the combined fit, while the second one is due to the variation of the lower bound from 0.5 GeV/c to 0.1 GeV/c for the pion spectrum.

	\sqrt{s}	$\langle\beta\rangle$	$T(\text{GeV})$	q_M	q_B	χ^2/NDF
TBW ($n = 1$)	0.9 TeV	$0.226 \pm 0.020 \pm 0.034$	$0.061 \pm 0.003 \pm 0.012$	$1.1278 \pm 0.0024 \pm 0.0078$	$1.0939 \pm 0.0026 \pm 0.0029$	67/94
	2.76 TeV	$0.193 \pm 0.012 \pm 0.042$	$0.086 \pm 0.001 \pm 0.009$	$1.1218 \pm 0.0005 \pm 0.0023$	$1.0989 \pm 0.0007 \pm 0.0004$	105/216
	5.02 TeV	$0.249 \pm 0.009 \pm 0.031$	$0.084 \pm 0.002 \pm 0.010$	$1.1260 \pm 0.0006 \pm 0.0025$	$1.1019 \pm 0.0007 \pm 0.0010$	163/231
	7 TeV	$0.262 \pm 0.009 \pm 0.042$	$0.086 \pm 0.002 \pm 0.013$	$1.1272 \pm 0.0006 \pm 0.0032$	$1.1025 \pm 0.0007 \pm 0.0005$	191/262
	13 TeV	$0.307 \pm 0.007 \pm 0.028$	$0.085 \pm 0.002 \pm 0.011$	$1.1306 \pm 0.0006 \pm 0.0029$	$1.1050 \pm 0.0006 \pm 0.0009$	238/265
TBW ($n = 0$)	0.9 TeV	$0.230 \pm 0.022 \pm 0.035$	$0.062 \pm 0.003 \pm 0.012$	$1.1284 \pm 0.0024 \pm 0.0078$	$1.0954 \pm 0.0024 \pm 0.0032$	68/94
	2.76 TeV	$0.200 \pm 0.013 \pm 0.045$	$0.086 \pm 0.002 \pm 0.010$	$1.1220 \pm 0.0005 \pm 0.0025$	$1.0993 \pm 0.0006 \pm 0.0008$	106/216
	5.02 TeV	$0.260 \pm 0.011 \pm 0.034$	$0.084 \pm 0.002 \pm 0.010$	$1.1265 \pm 0.0006 \pm 0.0027$	$1.1029 \pm 0.0007 \pm 0.0014$	167/231
	7 TeV	$0.271 \pm 0.010 \pm 0.046$	$0.087 \pm 0.002 \pm 0.012$	$1.1278 \pm 0.0006 \pm 0.0036$	$1.1036 \pm 0.0006 \pm 0.0013$	196/262
	13 TeV	$0.320 \pm 0.008 \pm 0.032$	$0.086 \pm 0.002 \pm 0.012$	$1.1314 \pm 0.0006 \pm 0.0034$	$1.1069 \pm 0.0005 \pm 0.0016$	252/265
BGBW	0.9 TeV	$0.272 \pm 0.016 \pm 0.066$	$0.142 \pm 0.004 \pm 0.028$	—	—	51/49
	2.76 TeV	$0.246 \pm 0.011 \pm 0.107$	$0.172 \pm 0.004 \pm 0.053$	—	—	36/59
	5.02 TeV	$0.277 \pm 0.010 \pm 0.104$	$0.171 \pm 0.004 \pm 0.055$	—	—	29/59
	7 TeV	$0.291 \pm 0.011 \pm 0.110$	$0.174 \pm 0.004 \pm 0.059$	—	—	34/59
	13 TeV	$0.329 \pm 0.013 \pm 0.108$	$0.174 \pm 0.005 \pm 0.059$	—	—	37/54

TABLE III. Summary of the freeze-out parameters for the TBW model at different multiplicity classes in pp collisions at 7 TeV. The explanation for the quoted errors is the same as those in Table II.

	Class	$\langle\beta\rangle$	$T(\text{GeV})$	q_M	q_B	χ^2/NDF
TBW ($n = 1$)	I	$0.437 \pm 0.004 \pm 0.018$	$0.087 \pm 0.002 \pm 0.015$	$1.1206 \pm 0.0008 \pm 0.0061$	$1.0937 \pm 0.0009 \pm 0.0025$	112/198
	II	$0.403 \pm 0.005 \pm 0.020$	$0.086 \pm 0.002 \pm 0.013$	$1.1227 \pm 0.0007 \pm 0.0052$	$1.0956 \pm 0.0008 \pm 0.0021$	110/198
	III	$0.369 \pm 0.005 \pm 0.025$	$0.087 \pm 0.002 \pm 0.014$	$1.1240 \pm 0.0007 \pm 0.0050$	$1.0965 \pm 0.0007 \pm 0.0017$	112/198
	IV+V	$0.333 \pm 0.006 \pm 0.030$	$0.086 \pm 0.002 \pm 0.013$	$1.1251 \pm 0.0006 \pm 0.0044$	$1.0978 \pm 0.0007 \pm 0.0013$	105/198
	VI	$0.283 \pm 0.009 \pm 0.040$	$0.086 \pm 0.002 \pm 0.013$	$1.1264 \pm 0.0006 \pm 0.0038$	$1.0997 \pm 0.0008 \pm 0.0007$	136/198
	VII	$0.241 \pm 0.011 \pm 0.043$	$0.084 \pm 0.002 \pm 0.011$	$1.1275 \pm 0.0006 \pm 0.0029$	$1.1007 \pm 0.0008 \pm 0.0001$	129/198
	VIII	$0.194 \pm 0.016 \pm 0.048$	$0.081 \pm 0.002 \pm 0.010$	$1.1288 \pm 0.0006 \pm 0.0022$	$1.1017 \pm 0.0009 \pm 0.0003$	149/197
	IX	0(fixed)	$0.080 \pm 0.001 \pm 0.004$	$1.1295 \pm 0.0006 \pm 0.0018$	$1.1044 \pm 0.0007 \pm 0.0018$	166/198
	X	0(fixed)	$0.060 \pm 0.002 \pm 0.007$	$1.1285 \pm 0.0008 \pm 0.0030$	$1.1008 \pm 0.0009 \pm 0.0031$	276/197
	TBW ($n = 0$)	I	$0.462 \pm 0.005 \pm 0.020$	$0.089 \pm 0.002 \pm 0.016$	$1.1242 \pm 0.0007 \pm 0.0069$	$1.1003 \pm 0.0007 \pm 0.0041$
II		$0.427 \pm 0.005 \pm 0.021$	$0.087 \pm 0.001 \pm 0.014$	$1.1254 \pm 0.0006 \pm 0.0058$	$1.1004 \pm 0.0006 \pm 0.0034$	104/198
III		$0.391 \pm 0.006 \pm 0.027$	$0.087 \pm 0.002 \pm 0.014$	$1.1259 \pm 0.0006 \pm 0.0055$	$1.1000 \pm 0.0006 \pm 0.0029$	107/198
IV+V		$0.351 \pm 0.007 \pm 0.032$	$0.087 \pm 0.002 \pm 0.014$	$1.1264 \pm 0.0006 \pm 0.0049$	$1.1003 \pm 0.0006 \pm 0.0024$	104/198
VI		$0.299 \pm 0.010 \pm 0.042$	$0.086 \pm 0.002 \pm 0.013$	$1.1272 \pm 0.0006 \pm 0.0042$	$1.1010 \pm 0.0007 \pm 0.0016$	135/198
VII		$0.254 \pm 0.012 \pm 0.046$	$0.084 \pm 0.002 \pm 0.012$	$1.1279 \pm 0.0006 \pm 0.0033$	$1.1015 \pm 0.0007 \pm 0.0008$	130/198
VIII		$0.202 \pm 0.017 \pm 0.052$	$0.081 \pm 0.002 \pm 0.010$	$1.1290 \pm 0.0006 \pm 0.0024$	$1.1021 \pm 0.0008 \pm 0.0002$	150/197
IX		0(fixed)	$0.080 \pm 0.001 \pm 0.004$	$1.1295 \pm 0.0006 \pm 0.0018$	$1.1044 \pm 0.0007 \pm 0.0018$	166/198
X		0(fixed)	$0.060 \pm 0.002 \pm 0.007$	$1.1285 \pm 0.0008 \pm 0.0030$	$1.1008 \pm 0.0009 \pm 0.0031$	276/197

TABLE IV. Summary of the freeze-out parameters for the TBW model at different multiplicity classes in pp collisions at 13 TeV. The explanation for the quoted errors is the same as those in Table II.

Class		$\langle\beta\rangle$	$T(\text{GeV})$	q_M	q_B	χ^2/NDF
TBW ($n = 1$)	I	$0.476 \pm 0.003 \pm 0.016$	$0.085 \pm 0.002 \pm 0.015$	$1.1234 \pm 0.0008 \pm 0.0066$	$1.0937 \pm 0.0008 \pm 0.0026$	118/200
	II	$0.440 \pm 0.004 \pm 0.020$	$0.087 \pm 0.001 \pm 0.015$	$1.1240 \pm 0.0006 \pm 0.0058$	$1.0954 \pm 0.0007 \pm 0.0023$	116/206
	III	$0.414 \pm 0.004 \pm 0.023$	$0.086 \pm 0.002 \pm 0.014$	$1.1258 \pm 0.0006 \pm 0.0053$	$1.0966 \pm 0.0007 \pm 0.0019$	127/206
	IV+V	$0.381 \pm 0.005 \pm 0.026$	$0.084 \pm 0.002 \pm 0.014$	$1.1279 \pm 0.0006 \pm 0.0046$	$1.0990 \pm 0.0007 \pm 0.0015$	132/206
	VI	$0.336 \pm 0.007 \pm 0.034$	$0.084 \pm 0.002 \pm 0.014$	$1.1289 \pm 0.0006 \pm 0.0042$	$1.1006 \pm 0.0007 \pm 0.0011$	165/205
	VII	$0.300 \pm 0.009 \pm 0.038$	$0.083 \pm 0.002 \pm 0.013$	$1.1299 \pm 0.0007 \pm 0.0035$	$1.1015 \pm 0.0008 \pm 0.0007$	190/205
	VIII	$0.259 \pm 0.012 \pm 0.040$	$0.081 \pm 0.002 \pm 0.011$	$1.1306 \pm 0.0007 \pm 0.0028$	$1.1022 \pm 0.0008 \pm 0.0003$	196/205
	IX	$0.196 \pm 0.019 \pm 0.035$	$0.076 \pm 0.002 \pm 0.006$	$1.1315 \pm 0.0007 \pm 0.0013$	$1.1039 \pm 0.0010 \pm 0.0002$	269/205
	X	0(fixed)	$0.062 \pm 0.001 \pm 0.006$	$1.1316 \pm 0.0008 \pm 0.0026$	$1.1033 \pm 0.0009 \pm 0.0024$	400/204
	TBW ($n = 0$)	I	$0.501 \pm 0.005 \pm 0.022$	$0.089 \pm 0.002 \pm 0.018$	$1.1277 \pm 0.0008 \pm 0.0080$	$1.1029 \pm 0.0007 \pm 0.0047$
II		$0.466 \pm 0.005 \pm 0.025$	$0.089 \pm 0.002 \pm 0.017$	$1.1275 \pm 0.0007 \pm 0.0068$	$1.1021 \pm 0.0006 \pm 0.0039$	134/206
III		$0.436 \pm 0.006 \pm 0.028$	$0.088 \pm 0.002 \pm 0.016$	$1.1284 \pm 0.0007 \pm 0.0062$	$1.1019 \pm 0.0006 \pm 0.0034$	146/206
IV+V		$0.399 \pm 0.006 \pm 0.031$	$0.086 \pm 0.002 \pm 0.015$	$1.1297 \pm 0.0006 \pm 0.0054$	$1.1029 \pm 0.0006 \pm 0.0028$	149/206
VI		$0.351 \pm 0.008 \pm 0.040$	$0.086 \pm 0.002 \pm 0.015$	$1.1300 \pm 0.0007 \pm 0.0049$	$1.1031 \pm 0.0007 \pm 0.0022$	177/205
VII		$0.312 \pm 0.011 \pm 0.044$	$0.084 \pm 0.002 \pm 0.014$	$1.1306 \pm 0.0007 \pm 0.0041$	$1.1032 \pm 0.0007 \pm 0.0016$	199/205
VIII		$0.267 \pm 0.013 \pm 0.046$	$0.082 \pm 0.002 \pm 0.012$	$1.1310 \pm 0.0007 \pm 0.0033$	$1.1033 \pm 0.0008 \pm 0.0010$	202/205
IX		$0.201 \pm 0.021 \pm 0.040$	$0.077 \pm 0.002 \pm 0.007$	$1.1317 \pm 0.0007 \pm 0.0015$	$1.1044 \pm 0.0009 \pm 0.0001$	271/205
X		0(fixed)	$0.062 \pm 0.001 \pm 0.006$	$1.1316 \pm 0.0008 \pm 0.0026$	$1.1033 \pm 0.0009 \pm 0.0026$	400/204

TABLE V. The values of $\langle dN_{\text{ch}}/d\eta \rangle$ at different multiplicity classes in pp collisions at 7 and 13 TeV. They are taken from Refs. [9, 10].

Class	7 TeV	13 TeV
I	21.3 ± 0.6	26.02 ± 0.35
II	16.5 ± 0.5	20.02 ± 0.27
III	13.5 ± 0.4	16.17 ± 0.22
IV+V	10.76 ± 0.3	12.91 ± 0.18
VI	8.45 ± 0.25	10.02 ± 0.14
VII	6.72 ± 0.21	7.95 ± 0.11
VIII	5.4 ± 0.17	6.32 ± 0.09
IX	3.9 ± 0.14	4.5 ± 0.07
X	2.26 ± 0.12	2.55 ± 0.04

TABLE VI. The values of $\langle dN_{\text{ch}}/d\eta \rangle$ at different centralities in Pb-Pb (Pb-Pb, Xe-Xe, p-Pb) collisions at 2.76 (5.02, 5.44, 5.02) TeV. They are taken from Refs. [6–8, 64].

Centrality	0-10%	10-20%	20-40%	40-60%	60-80%
Pb-Pb 2.76 TeV	1447.5 ± 54.5	966 ± 37	537.5 ± 19	205 ± 7.5	55.5 ± 3
Pb-Pb 5.02 TeV	1765 ± 51.5	1180 ± 31	649 ± 17.5	250.5 ± 10	70.6 ± 4.6
p-Pb 5.02 TeV	40.6 ± 0.9	30.5 ± 0.7	23.2 ± 0.5	16.1 ± 0.4	9.8 ± 0.2
Centrality	0-10%	10-30%	30-50%	50-70%	70-90%
Xe-Xe 5.44 TeV	1053 ± 25	592 ± 14	256.5 ± 6.5	91.35 ± 2.5	22.65 ± 1.1